Coke Combustion and Gasification Kinetics in Ethane Steam Crackers

G. J. Heynderickx, E. M. Schools, and G. B. Marin
Laboratorium voor Petrochemische Techniek, Universiteit Gent, B9000 Gent, Belgium

DOI 10.1002/aic.10401
Published online March 21, 2005 in Wiley InterScience (www.interscience.wiley.com).

A simulation model for the development of the optimal decoking procedure of a steam cracker is constructed. It is based on experimental data for the process gas side coke combustion with oxygen and the process gas side coke gasification with steam, using coke samples taken from an industrial steam cracker. The texture changes of the coke during the combustion and gasification are accounted for. Different kinetic models are combined with a coke porosity model and different gas–solid reaction/diffusion models. The model parameters are estimated from the experimental data and model discrimination is performed. For the coke combustion the kinetic model is based on the dissociative chemisorption of oxygen on the active coke sites, whereas a general gas–solid reaction/diffusion model is required. The growth of the pores and the overlap of the pores during the coke combustion are found to compensate each other. For the coke gasification, the kinetic mechanism is based on the dissociative chemisorption of steam, whereas a uniform gas–solid reaction/diffusion model is used. © 2005 American Institute of Chemical Engineers
AIChE J, 51: 1415–1428, 2005
Keywords: coke combustion, coke gasification, steam cracking, kinetic model, reaction/diffusion model

Introduction

Thermal cracking of hydrocarbons to olefins is an endothermal process carried out in tubular reactor coils suspended in large gas-fired furnaces. Undesired side reactions during the thermal cracking process result in the formation of coke on the internal tube skin of the reactor coils. The growing coke layer results in a growing pressure drop over the reactor coil, which negatively influences the ethylene selectivity of the cracking, and in a higher heat transfer resistance requiring more furnace firing and higher external tube skin temperatures to maintain the process gas conversion. Finally, the furnace is taken out of production to remove the coke layer by a controlled burning with a mixture of steam and air. The decoking process is a very sensitive process: local peaks in tube skin temperatures can result in tube damage. Although rigorous simulation software is available to calculate the cracking process[1-4] and the corresponding coke formation,[5-10] simulation models to describe the decoking process are less detailed and do not allow optimization of the decoking procedure of a thermal cracking unit. In this paper an accurate and detailed model is developed and presented, based on extended experimental work and on detailed models describing the gas–solid reaction kinetics, the solid-phase changes during reaction, the diffusion of the gas components through the pores of the coke layer, and the diffusion of the components through the laminar layer between the coke layer and the turbulent process gas bulk flow.

To be able to select an accurate model to describe the gas–solid interaction, a physicochemical characterization of the coke formed during the thermal cracking process is needed. This not only will lead to more complete insight into the complex phenomena and mechanisms of the coke formation, but will also be of use for the description of the different reactions taking place during the decoking process. It is important to realize that the activity of the coke in the presence of oxygen and steam is determined, not only by the reaction

Correspondence concerning this article should be addressed to G. B. Marin at guy.marin@UGent.be.

conditions such as temperature and partial pressures, but also by the porosity of the coke, possibly by the metals content of the coke, and by their evolution during the decoking process. In particular, the porous structure will directly influence the decoking rate because oxygen and steam have to diffuse through the pores of the coke and consequently react at an active site on the internal coke surface area. Furthermore, because of the consumption of the coke in the decoking reactions, the porous structure of the coke will change continuously. A complete decoking model has to take into account all these phenomena.

An experimental setup is developed to study the decoking process. The combustion of coke with oxygen, on the one hand, and the gasification of coke with water vapor, on the other hand, are studied separately. This is necessary because there is a large difference in reaction rate of both decoking reactions. Different kinetic models are combined with a coke porosity model and with different gas–solid reaction/diffusion models. The model parameters are estimated from the experimental data and a model discrimination is performed.

Experimental

Physicochemical characterization of the coke

The experimental work is carried out with coke from an industrial ethane cracking furnace that had an emergency shutdown after 25 days of operation. The coke samples are taken from the last U-turn of the reactor coil near the bottom of the furnace. Previous work[11-14] has shown that the thickest coke layer is formed at that position because the tube skin temperatures reach their highest values in the last U-turn. The coke layer samples used in this work are 5.5 mm thick.

During the experimental research, a distinction is made between the coke formed directly on the internal tube skin (tube metal side coke) and the coke formed at the process gas side (process gas side coke).

The morphology of the coke is studied using scanning electron microscopy (SEM) and X-ray diffraction (XRD). The chemical composition of the coke is determined using energy-dispersive analysis of X-rays (EDAX). The textural characterization (that is, porosity, internal pores surface area, density, etc.) of the coke is done with adsorption and desorption measurements of liquid N_2, Hg-porosimetry, and picnometry. SEM shows that the tube metal side coke and the process gas side coke have a different morphology. The tube metal side coke mainly has the form of filaments or globes; the process gas side coke has a porous, layered structure. This corresponds with the observations of Bennett and Price,[15] Kim et al.,[16] and Albright and Marek.[17-19]

The XRD study of the coke reveals that the tube metal side coke has a more crystalline structure and is more graphitized than the process gas side coke. This is attributed to the graphitizing process as described by Marchand.[20] The XRD results correspond with those of Bennet and Price,[15] Jackson et al.,[21] and Marchand.[20]

From EDAX measurements, it is found that process gas side coke contains negligible amounts of metals and inorganic impurities. The tube metal side coke, especially the filaments, contains a large amount of metals, corresponding with the filament-growing mechanism as reported by Baker et al.,[22,23] Bernardo and Lobo,[24] and Figueiredo.[25] For further details on coke formation mechanisms and kinetics, reference is made to Lahaye et al.,[26] Kopinke et al.,[5,6] Reyniers et al.,[7] Wauters and Marin,[8,9] and Van Speybroeck et al.[10]

Table 1. Textural Characterization of Porous Layer Coke

Parameter	Porous Layer (This Work)	Bennet and Price (1981)	Trimm (1977)
$p_{t,0}$ (kg C_0 m_s^{-3})	1860	1870	1880
$\rho_{p,0}$ (kg C_0 m_p^{-3})	1675	1664	1560
$S_{m,0}$ (m_s^2 kg C_0^{-1})	350	140	2300
$\varepsilon_{s,0}$ (m_f^3 m_p^{-3})	0.10	0.12	0.17

The results on the texture study are summarized in Table 1 and compared with the results of Bennet and Price[15] and Trimm.[27] A porosity of 0.1 m_f^3 m_p^{-3} corresponds with the values determined from the SEM study. The coke is found to be macroporous. The amount of meso- and micropores is negligible.

Procedure and data

Equipment. The kinetic data were obtained with the experimental setup presented in Figure 1. In an industrial thermal cracking process, tubular reactors working under integral conditions are used. Such a reactor type is not particularly suitable for a kinetic study because of the temperature and pressure profile along the reactor, resulting in the measurement of averaged decoking rates only.

An experimental recycle reactor operating under conditions of complete mixing is constructed primarily for the study of the combustion of process gas side coke with oxygen. The same setup is used for a separate, but limited, study of the gasification of process gas side coke with steam. From the experimental study of Bennett and Price[28] it was found that the steam gasification of coke becomes significant only at temperatures > 850°C. At that temperature the combustion rate of coke is extremely high. The experimental study in this work shows that the steam gasification of coke slowly starts at temperatures > 880°C. Because the experimental setup was not developed to withstand such high temperatures, only very few steam gasification experiments are conducted. The following discussion of the procedure and data is done from the perspective of the combustion experiments. An analogous discussion can be developed from the perspective of the gasification experiments.

A limited number of experiments are done with tube metal side coke; they are not used to determine the decoking kinetics.

The coke samples from the industrial cracking unit are fractured into particles with a diameter of 1 to 1.2 mm. For a combustion experiment, 60 to 200 mg of particles are put in a small basket that is suspended on the arm of an electrobalance, allowing a direct and continuous measurement of the coke mass in the basket as a function of time. The process gas is continuously recycled and the recycle-to-feed flow ratio is maintained sufficiently high to establish complete mixing. The decoking reaction progresses at a unique concentration level (that is, the composition of the outlet flow) while isothermal conditions are attained. Step-response experiments are performed to determine the influence of different operation conditions [rotor speed (rpm), inlet feed flow, composition of process gas, and reaction temperature] on the presence or the absence of complete mixing in the reactor. It was established that the rotor speed

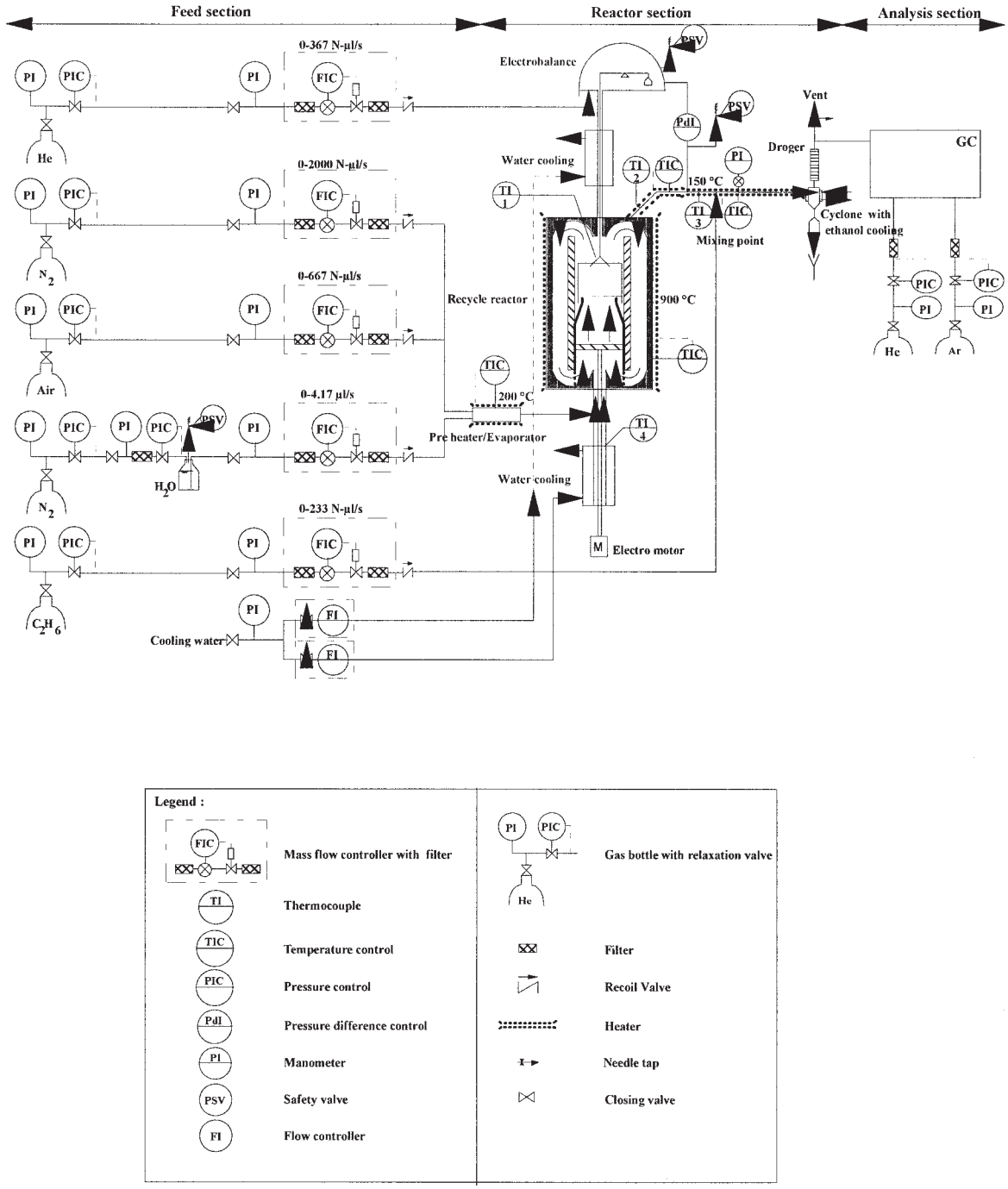

Figure 1. Experimental setup.

should be >9000 rpm, the coke sample mass in the basket <100 mg, and the O_2 conversion level limited to 75% to have complete mixing, as discussed more extensively in the following paragraph. High coke conversion and high reaction temperatures are possible while the consumption of gases is low. The process gas velocity is sufficiently high to allow neglecting of external mass and heat transport limitations, as will be shown.

Data Acquisition and Parameter Estimation. The reactor effluent is analyzed with a Chrompack CP9001 gas chromatograph with a TCD detector. Two channels are used. In the first channel He is used as the carrier gas and CO_2, C_2H_6 (internal standard), O_2, N_2, CH_4, and CO are determined. In the second channel Ar is used as a carrier gas and H_2 and He are detected. The analysis of a gas sample takes about 25 min.

One experiment takes from 7 to 12 h and the number of analyses per experiment varies between 8 and 15. The mass of the coke in the basket is measured every second. The total number of experiments amounts to 37 for the combustion of process gas side coke with oxygen and two for the gasification of process gas side coke with steam.

The calibration factors for the different components *i* are

calculated using a reference component (N_2), and using different calibration mixtures, as follows:

$$CF_i = \frac{w_i}{w_{ref}} \frac{A_{ref}}{A_i} \tag{1}$$

The conversion of the coke at a given time is calculated from

$$X_C(t) = \frac{W_{C,0} - W_C(t)}{W_{C,0}} \tag{2}$$

for the process gas side coke.

The total coke combustion rate, based on the initial coke mass in the basket, is calculated from

$$R_{C+O_2}(t) = \frac{dX_C(t)}{dt} = -\frac{1}{W_{C,0}} \frac{dW_C(t)}{dt} \tag{3}$$

The specific coke combustion rate, based on the actual coke mass in the basket at a given time t, is calculated from

$$R'_{C+O_2}(t) = \frac{1}{1 - X_C(t)} \frac{dX_C(t)}{dt} = -\frac{1}{W_C(t)} \frac{dW_C(t)}{dt} \tag{4}$$

The mass flow rate of each component in the reactor effluent is calculated from

$$\dot{m}_i(t) = \frac{CF_i}{CF_{C_2H_6}} \frac{A_i(t)}{A_{C_2H_6}(t)} \dot{m}_{C_2H_6} \tag{5}$$

The use of the internal standard ethane enabled us to calculate the outlet flow rates and to verify the total mass balance for each experiment. The molar flow rates are determined from the mass flow rates:

$$F_i(t) = \frac{\dot{m}_i(t)}{M_i} \tag{6}$$

The oxygen consumption rate is then calculated from

$$F_{O_2,0} - F_{O_2}(t) - R_{O_2}(t) W_{C,0} = V_r \frac{dC_{O_2}(t)}{dt} \tag{7}$$

whereas the rate of formation of component i is given by

$$-F_i(t) - R_i(t) W_{C,0} = V_r \frac{dC_i(t)}{dt} \tag{8}$$

with

$$C_i(t) = \frac{p_i(t)}{RT} = \frac{F_i(t)}{\Sigma_i F_i(t)} p_t \tag{9}$$

The accumulation contribution in the right-hand side of Eqs. 7 and 8 was found to be negligible: the gas phase concentrations almost immediately adapt to the gas–solid reactions in the coke particle. The consumption rate of oxygen is calculated from

$$R_{O_2} = \frac{F_{O_2,0} - F_{O_2}(t)}{W_{C,0}} = \frac{F_{O_2,0}}{W_{C,0}} X_{O_2}(t) \tag{10}$$

and the reaction rate can be explicitly determined from the measured conversion. From the rates of formation of CO and CO_2, the selectivity is calculated from

$$S_i(t) = -\frac{R_i(t)}{R_{O_2}(t)} \tag{11}$$

When determining the range of operating conditions for the experiments, the possibility of transport limitations during the experiments has to be examined and, if needed, accounted for. The global rate of coke combustion equals the intrinsic rate of coke combustion only if there are no transport limitations. Therefore, the reaction conditions at which transport limitations occur are examined. For the external transport limitations, both experimental and theoretical assessments were performed. Internal transport limitations were evaluated only theoretically.

The experimental verification on external transport limitations was performed by varying the rotor speed. A higher rotor speed gives a thinner laminar boundary layer around the coke particles in the basket and thus a lower resistance against mass and heat transfer. A rotor speed of 9000 rpm is found to be the critical value for transport limitations. A theoretical calculation of the concentration and temperature drop over the laminar film at 9800 rpm, with the mass transfer coefficient calculated from the Sherwood number determined with an empirical correlation for a packed bed,[29,30]

$$\mathrm{Sh} = 2 + 1.1\mathrm{Re}^{0.6}\mathrm{Sc}^{0.33} \tag{12}$$

and the heat transfer coefficient calculated from a Nusselt number based on an empirical correlation for a packed bed[31]

$$\mathrm{Nu} = 2 + 1.1\mathrm{Re}^{0.6}\mathrm{Pr}^{0.33} \tag{13}$$

resulted in $\Delta C_{film} = 0.0059$ mol m_f^{-3} and $\Delta T_{film} = 4.6$ K. These differences are negligible under the given operating conditions.

For the theoretical verification on the absence of internal mass transport limitations, use was made of the Weisz–Prater[32] criterion:

$$\Phi = \frac{R_{O_2} \rho_{p,0} L_0^2}{D_{e,O_2} (C_{O_2})_s^s} \ll 1 \tag{14}$$

The calculation of the effective diffusivity of the oxygen in the pores is discussed in the modeling section. It is found that, for temperatures < 580°C, there are no internal mass transport limitations, regardless of the diameter of the pores. With rising temperature, the net consumption rate of oxygen is gradually influenced to a greater degree by the diffusion of oxygen through the pores. From 650°C on, mass transport limitations are to be accounted for in all pore sizes. The maximal internal

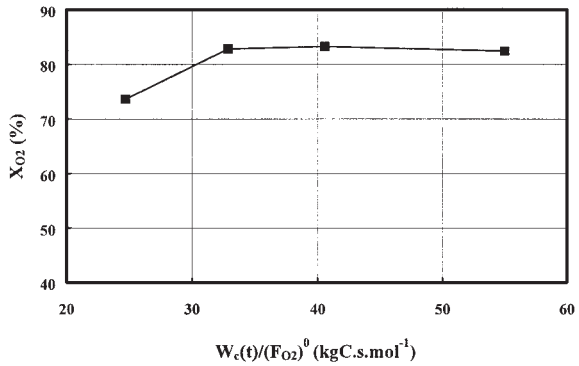

Figure 2. Oxygen conversion as a function of space–time at 800°C.

$X_C = 0.2$, $(p_{O2})^0 = 4.5$ kPa.

temperature gradient over the coke particles is calculated from[33]

$$\Delta T_{\max} = \frac{(-\Delta H) D_{e,O_2} C_{O_2}}{\lambda_C} \tag{15}$$

At 740°C, the calculated temperature difference over the particle is <0.01°C. It is concluded that internal heat transfer limitations need not be accounted for under the given operating conditions.

A last criterion that is used when determining the range of operating conditions is confirmation of complete mixing at all operating conditions. From Figure 2 it follows that the oxygen conversion during the experiments does not reach 100%. This is explained by the finite recycling rate and a limited bypass of the basket containing the coke particles in the recycle reactor. By limiting the oxygen conversion to about 75%, complete mixing during the experiments is guaranteed. The investigated range in experimental conditions for the process gas side coke combustion is summarized in Table 2.

Parameter estimations are performed using a Levenberg–Marquardt algorithm incorporated into an in-house written code.[34] The sum of squares of the difference between the observed and the calculated coke conversion is minimized by adjusting the model parameter vector $\bar{b}$, which is expected to approach the real parameter vector $\bar{\beta}$ when the optimum is reached:

$$SSQ = \sum_{i=1}^{n} \sum_{j=1}^{m_i} [X_{C,ij}(t) - \hat{X}_{C,ij}(t)]^2 \overset{\bar{b}}{\rightarrow} MIN \tag{16}$$

where n is the number of experiments and m_i is the number of sample measurements for experiment i.

The statistical significance of the global regression is expressed by means of the so-called F-test, which is based on the comparison of the calculated sum of squares of the calculated response value and the residual sum of squares (SSQ). A high F-value corresponds with a high significance of the global regression. The parameter estimates are also tested for statistical significance on the basis of their individual t-values, which are related to the sensitivity of the model calculations on the values of the individual parameters. A high t-value corresponds with a high sensitivity and, thus, a high significance or a narrow (95%) approximate individual confidence interval for the corresponding parameter.

Model Construction

As discussed earlier in the introduction, the combustion and the gasification of coke are examined and modeled separately.

Coke combustion

The experimental data provide information on the overall combustion rate of the coke particles, which is determined by the intrinsic combustion rate of oxygen on the active carbon sites situated on the internal coke surface, on one hand, and by the mass transport of oxygen and the combustion products in the pores of the coke particle, on the other hand. To describe this mass transport through the pores, the internal mass diffusion limitations have to be modeled as well. For the intrinsic combustion rate of oxygen, three kinetic models are proposed. They are combined with three gas–solid reaction/diffusion models: a uniform, a heterogeneous, and a general model. Typical partial pressure profiles are presented in Figure 3. The change of the pores during the combustion is incorporated by introducing a texture model.

During combustion, the coke particles react with oxygen to form carbon oxide and carbon dioxide according to the following heterogeneous gas–solid reactions:

$$C + \frac{1}{2} O_2 \rightarrow CO \tag{17}$$

$$C + O_2 \rightarrow CO_2 \tag{18}$$

The carbon oxide reacts to carbon dioxide according to the homogeneous gas phase reaction:

$$CO + \frac{1}{2} O_2 \rightarrow CO_2 \tag{19}$$

By means of the Boudouard reaction, carbon dioxide reacts with coke to form carbon oxide:

$$C + CO_2 \leftrightarrow 2CO \tag{20}$$

The latter reaction is much slower than the combustion reactions and can be ignored in the modeling of the coke combustion. Typical profiles for oxygen, carbon oxide, and carbon dioxide are given in Figure 4. These profiles are consistent with

Table 2. Range of Experimental Conditions for Coke Combustion Experiments

N (rpm)	9500–9800
$W_{C,0}$ (10^{-6} kg C_0)	60
T (°C)	650–740
$W_{C,0}/(F_{O_2})^0$ (kg C_0 s mol^{-1})	27–91
$(p_{O_2})^0$ (kPa)	2.1–8.5
X_{O_2} (%)	<75
F' (N · μL s^{-1})	<1000

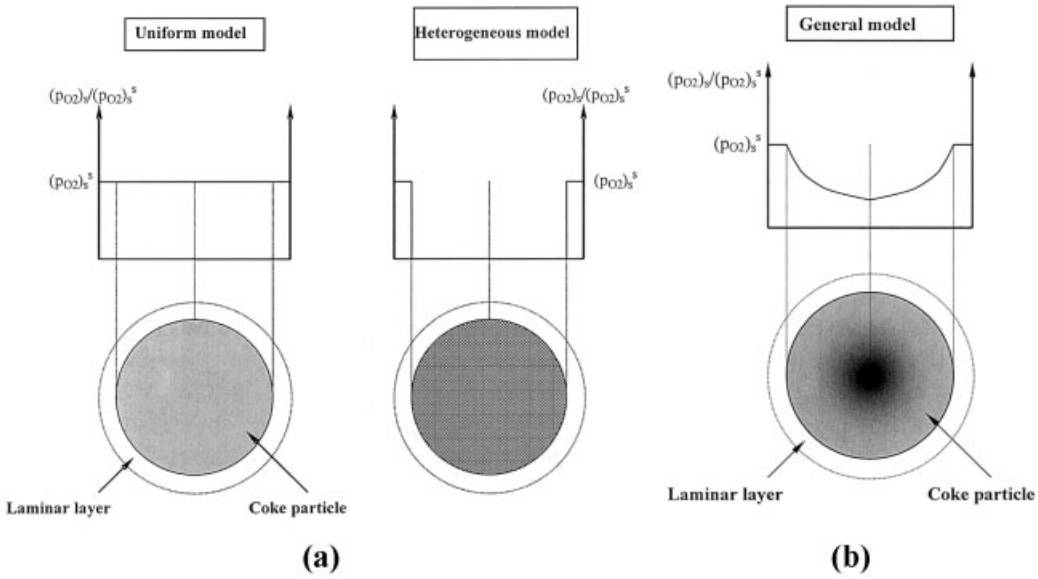

Figure 3. Oxygen particle pressure profiles of gas–solid reaction/diffusion models.

(a) Uniform model vs. heterogeneous model; (b) general model.

the following reaction network: the coke combustion mainly proceeds through reaction 18, whereas the small amount of carbon oxide formed through reaction 17 directly reacts according to reaction 19. From this, it follows that

$$R_{O_2} = R_{CO_2} = \frac{R_{C+O_2}}{M_C} \tag{21}$$

which is confirmed in Figure 5.

The total and specific combustion rates, as a function of coke conversion, are shown in Figure 6. These rates are influenced by diffusional limitations in the pores and represent global, not intrinsic, rates. The evolution of both curves in Figure 6 is a consequence of the textural changes of the porous coke particles during combustion. Textural parameters, such as porosity, specific surface area, and pore diameter distribution, change during the combustion of the coke, resulting in a changing number of active carbon sites. This is confirmed by SEM measurements. The pores grow with rising conversion, resulting in an increase of the total internal pores surface area and of the number of active carbon sites. On the other hand, the SEM measurements also show that the growth of the pores results in overlap of the pores, giving a reduction of the total internal surface area and of the number of active sites. From the maximum in the total combustion rate profile in Figure 6, it can be concluded that the latter phenomenon dominates from a coke conversion of 20% on. The measured profiles are typical for gas–solid reactions with diffusional limitations in the pores of the solid material, such as coke combustion.[35] The textural changes mainly occur in a reaction zone, moving gradually through the solid as a function of time. Because the evolution of the internal surface area of the pores was not determined independently in this research, a texture model was incorporated in the model equations used for the regression of experimental data. Furthermore, from the smoothness of the profiles shown in Figure 6, it can also be concluded that fracture of the coke particles does not occur during the experiments.

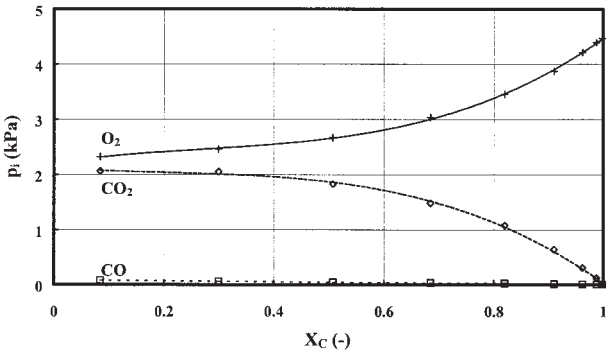

Figure 4. Partial pressure profiles in reactor effluent as a function of coke conversion in coke combustion.

T = 700°C, $(p_{O2})^0$ = 4.5 kPa, $W_{C,0}/(F_{O2})^0$ = 38.5 kg C_0 s mol^{-1}.

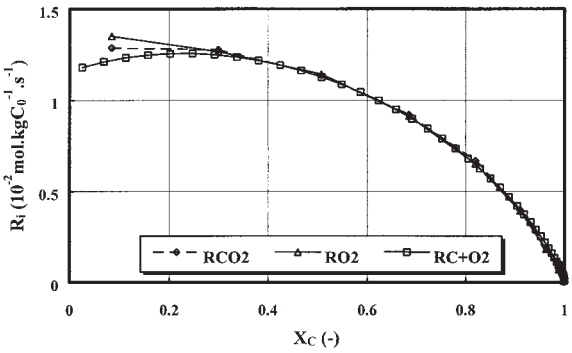

Figure 5. Rate of combustion/formation of oxygen, coke, and carbon dioxide as a function of coke conversion in coke combustion.

T = 700°C, $(p_{O2})^0$ = 4.5 kPa, $W_{C,0}/(F_{O2})^0$ = 38.5 kg C_0 s mol^{-1}.

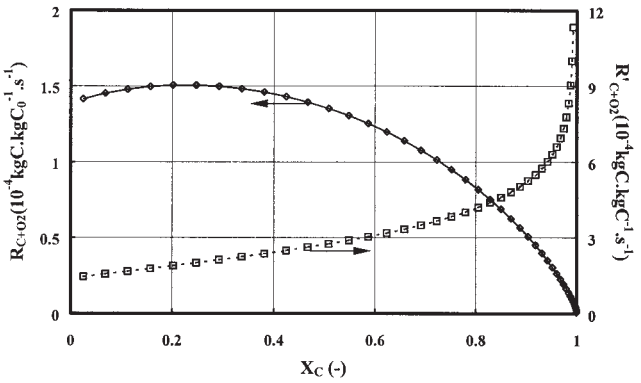

Figure 6. Total and specific rate of coke combustion as a function of coke conversion.

T = 700°C, $(p_{O2})^0$ = 4.5 kPa, $W_{C,0}/(F_{O2})^0$ = 38.5 kg C_0 s mol^{-1}.

Texture Model. The incorporation of a texture model proceeds along the following lines. The specific combustion rate of the coke is calculated from

$$R'_{C+O_2}(t) = \frac{1}{1 - X_C(t)} \frac{dX_C(t)}{dt} = f(p_{O_2}, T) C_t(X_C) \quad (22)$$

whereas the total combustion rate is then determined by

$$R_{C+O_2}(t) = \frac{dX_C(t)}{dt} = f(p_{O_2}, T) C_t(X_C)[1 - X_C(t)] \quad (23)$$

The specific number of active carbon sites is calculated from

$$C_t(X_C) = \lambda(X_C) S_m(X_C) \quad (24)$$

transforming Eq. 22 into

$$R'_{C+O_2}(t) = \frac{1}{1 - X_C(t)} \frac{dX_C(t)}{dt} = [f(p_{O_2}, T) C_{t,0}] \frac{\lambda(X_C) S_m(X_C)}{\lambda_0 S_{m,0}} \quad (25)$$

Given that the graphitizing process of coke is much slower than the decoking run time of a cracker unit,[36] the degree of graphitization of the coke, and thus the number of active coke sites per unit surface area, is assumed to remain constant during the coke combustion:

$$R'_{C+O_2}(t) = \frac{1}{1 - X_C(t)} \frac{dX_C(t)}{dt} = [f(p_{O_2}, T) C_{t,0}] \frac{S_m(X_C)}{S_{m,0}} \quad (26)$$

Furthermore

$$S_m(X_C) = \frac{S_V(X_C)}{\rho_p(X_C)} = \frac{S_V(X_C)}{\rho_{t,0}(1 - \varepsilon_{s,0})(1 - X_C)} \quad (27)$$

and, in particular, at the start of the decoking operation

$$S_{m,0} = \frac{S_{V,0}}{\rho_{p,0}} = \frac{S_{V,0}}{\rho_{t,0}(1 - \varepsilon_{s,0})} \quad (28)$$

resulting in

$$\frac{S_m(X_C)}{S_{m,0}} = \frac{1}{1 - X_C} \frac{S_V(X_C)}{S_{V,0}} \quad (29)$$

Finally, by combining the above equations, the total combustion rate is expressed as

$$R_{C+O_2}(t) = \frac{dX_C(t)}{dt} = [f(p_{O_2}, T) C_{t,0}] \frac{S_V(X_C)}{S_{V,0}} \quad (30)$$

The contribution $S_V(X_C)/S_{V,0}$ can be determined directly when a heterogeneous gas–solid reaction/diffusion model (Figure 3) is used. With this heterogeneous model, the coke only reacts at the outer particle surface and

$$\frac{S_V(X_C)}{S_{V,0}} = \left(\frac{d_p}{d_{p,0}}\right)^2 \quad (31)$$

for spherical particles. Taking into account

$$X_C(t) = 1 - \frac{W_C(t)}{W_{C,0}} = 1 - \left(\frac{d_p}{d_{p,0}}\right)^3 \quad (32)$$

Equation 31 is transformed into

$$\frac{S_V(X_C)}{S_{V,0}} = [1 - X_C(t)]^{2/3} \quad (33)$$

When a uniform or a general gas–solid reaction/diffusion model (Figure 3) is used, the coke reacts in the entire particle and the contribution $S_V(X_C)/S_{V,0}$ is calculated from a texture model.

Different types of texture models are available in literature.

Grain models were reported by the following investigators: Szekely and Evans[37,38]; Sohn and Szekely[39,40]; Park and Levenspiel[41]; Szekely and Propster[42]; Adschiri and Furusawa[43]; Adschiri et al.[44]; and Sotirchos.[45]

Pore models or capillary models were reported by Petersen,[46] Hashimoto and Silveston,[47] Simons and Finson,[48] and Simons.[49,50] Bhatia and Perlmutter[51] and Gavalas[52] reported, independently, the pore model that is used in this work:

$$\frac{S_V(X_C)}{S_{V,0}} = (1 - X_C)\sqrt{1 - \Psi \ln(1 - X_C)} \quad (34)$$

introducing a single texture parameter Ψ:

$$\Psi = 4\pi \frac{L_{m,0}}{S_{m,0}^2 \rho_{t,0}} \quad (35)$$

This model is mathematically derived based on the assumptions that the pores are cylindical, are randomly scattered, have

a random pore size distribution, grow with a constant rate, and are all accessible. The volume of the particle is assumed to remain invariant during the reaction and the particle is assumed to be isothermal.

Other pore models were reported by Sotirchos[45] and Delikouras and Perlmutter.[53,54]

A third type of pore model constitutes the percolation models,[55,56] introduced by Shah and Ottino,[57] Fuertes and Marban,[58] and Marban and Fuertes.[59]

Kinetic Model. Several reaction mechanisms and corresponding reaction kinetics for coke combustion have been reported in literature.

A first group of mechanisms is based on the dissociative chemisorption of oxygen on the active carbon sites. The simplest mechanism was presented by Laine et al.[60]:

$$C_{fs} + \frac{1}{2}\,O_2 \xrightarrow{k_{a,d,O_2}} C(O) \tag{36}$$

$$C(O) \xrightarrow{k_{sr,d,O_2}} CO + C_{fs} \tag{37}$$

Oxygen is chemisorbed in a dissociative manner. The chemisorption is irreversible and a semiquinon group is formed. The corresponding kinetic expression is deduced under the assumption that the specific number of active carbon sites at a given coke conversion is constant. This specific number of active carbon sites is obtained by summing up the free active coke sites and the number of surface intermediates:

$$C_t(X_C) = C_{fs} + C(O) \tag{38}$$

Furthermore, the pseudo-steady state is assumed for the surface intermediates, resulting in

$$R'_{C+O_2}(t) = \frac{k_{a,d,O_2}\sqrt{p_{O_2}}\;C_t(X_C)}{1 + \dfrac{k_{a,d,O_2}}{k_{sr,d,O_2}}\sqrt{p_{O_2}}} \tag{39}$$

Other mechanisms based on the dissociative chemisorption of oxygen were reported by Blyholder and Eyring,[61] Laurendeau,[62] Chen et al.,[63] and Li et al.[64] The latter mechanisms have a different degree of sophistication. Some consider, for instance, the migration of adsorbed species over the coke surface.

A second group of mechanisms is based on the molecular chemisorption of oxygen with the formation of unstable semiquinon groups. Such a mechanism was introduced by Essenhigh[65] and Walker et al.,[66] as follows:

$$C_{fs} + O_2 \xrightarrow{k_{a,m,O_2}} C(O_2) \tag{40}$$

$$C(O_2) \xrightarrow{k_{sr,m,O_2}} CO_2 + C_{fs} \tag{41}$$

Under the same assumptions as described above, the corresponding specific rate equation becomes

$$R'_{C+O_2}(t) = \frac{k_{a,m,O_2}p_{O_2}C_t(X_C)}{1 + \dfrac{k_{a,m,O_2}}{k_{sr,m,O_2}}\,p_{O_2}} \tag{42}$$

A similar mechanism, but considering surface migration as well, was considered by Du et al.[67,68]

A third group of mechanisms considers both types of oxygen chemisorption,[66] leading to

$$R'_{C+O_2}(t) = \frac{(k_{a,d,O_2}\sqrt{p_{O_2}} + k_{a,m,O_2}p_{O_2})C_t(X_C)}{1 + \dfrac{k_{a,d,O_2}}{k_{sr,d,O_2}}\sqrt{p_{O_2}} + \dfrac{k_{a,m,O_2}}{k_{sr,m,O_2}}\,p_{O_2}} \tag{43}$$

The rate equations for all the proposed mechanisms can finally be grouped into three model categories.

(1) Model I: Dissociative oxygen chemisorption

$$R'_{C+O_2}(t) = \frac{k_1\sqrt{p_{O_2}}\;C_t(X_C)}{1 + k_2\sqrt{p_{O_2}}} \tag{44}$$

(2) Model II: Associative oxygen chemisorption

$$R'_{C+O_2}(t) = \frac{k_3p_{O_2}C_t(X_C)}{1 + k_4p_{O_2}} \tag{45}$$

(3) Model III: Dissociative and associative oxygen chemisorption

$$R'_{C+O_2}(t) = \frac{(k_1\sqrt{p_{O_2}} + k_3p_{O_2})C_t(X_C)}{1 + k_2\sqrt{p_{O_2}} + k_4p_{O_2}} \tag{46}$$

In these models, the activation energy and the preexponential factors are to be estimated from the experimental data, together with the texture parameter Ψ, when the texture model Eq. 34 is needed, that is, when the uniform or general gas–solid reaction/diffusion model is applied.

Parameter Estimation and Model Discrimination. The parameter estimation using Eq. 16 requires the calculation of the coke conversion arising from combustion:

$$\frac{d\hat{X}_C(t)}{dt} = R_{C+O_2}(t) = R'_{C+O_2}(t)[1 - \hat{X}_C(t)] \tag{47}$$

with the total combustion rate given by Eq. 30, using Eq. 33 or Eq. 34 to determine the textural changes, and using the specific combustion rate calculated with one of the models expressed in Eqs. 44, 45, and 46.

The parameter estimation proceeds following two consecutive steps.

To obtain good initial parameter estimates in the first of the two consecutive steps, the kinetic model is combined with (Figure 3)

- a uniform gas–solid reaction/diffusion model
- a heterogeneous gas–solid reaction/diffusion model

Table 3. Estimated Parameter Values and Corresponding 95% Confidence Intervals*

Gas–Solid Reaction/Diffusion Model	Uniform	Heterogeneous	General
Kinetic model	II	II	I or II
$k_1 C_{t0}$			
A^* (10^{-4} s^{-1} kPa$^{-0.5}$)	—	—	4.0308 ± 0.2803
$E_{a,1}$ (J mol^{-1})	—	—	121,399 ± 16,185
k_2			
A^* (kPa$^{-0.5}$)	—	—	0.59471 ± 0.0914
$E_{a,2}$ (J mol^{-1})	—	—	−168,863 ± 28,300
$k_3 C_{t0}$			
A^* (10^{-4} s^{-1} kPa^{-1})	2.0090 ± 0.0407	1.9871 ± 0.08281	8.5298 ± 0.8378
$E_{a,3}$ (J mol^{-1})	65,689 ± 13,646	65,705 ± 14,353	135,417 ± 35,125
k_4			
A^* (kPa^{-1})	0.49662 ± 0.0367	0.51436 ± 0.04641	2.2656 ± 0.2763
$E_{a,3}$ (J mol^{-1})	−134,165 ± 28,645	−129,746 ± 28,134	−83,851 ± 43,350
Ψ	0.76845 ± 0.18706	—	0

*Experiments at all temperatures used: $T_{avg} = 717°C$; $A^* = A \exp(-E/RT_{avg})$. Kinetic models: I, dissociative O_2 chemisorption; II, associative O_2 chemisorption.

When the uniform model is used, internal diffusion limitations are neglected: the oxygen partial pressure in the pores of the coke particle is equal to the partial pressure of the oxygen in the bulk gas flow, that is, the diffusional rate is infinitely fast compared to the combustion rate. Reaction occurs all over the coke particle and a texture model (Eq. 34) is needed. When the heterogeneous model is used, the combustion reactions are assumed to occur at the external particle surface only and Eq. 33 can be used. The oxygen partial pressure in the particle is assumed to be zero, that is, the combustion rate is infinitely fast compared to the diffusional rate.

Equation 47 is used with both approaches to calculate the coke conversion. The kinetic model based on the associative oxygen chemisorption (Eq. 45) is found to give the best fit between experimental and calculated data. The kinetic models based on the dissociative chemisorption of oxygen and based on the dissociative and associative chemisorption of oxygen are rejected because significantly negative rate coefficients are obtained. The estimated parameter values are given in Table 3. Note that a negative apparent activation energy indicates that the activation energy for the desintegration of the complex is larger than that of the chemisorption step.

The final parameter estimates are determined in a second step, in which reaction and diffusion are considered using a general model for gas–solid interactions (Figure 3), taking into account an oxygen partial pressure concentration gradient in the pores, that is, taking into account the correct internal mass transport limitations. As discussed earlier, internal and external heat transport limitations as well as external mass transport limitations can be neglected.

A detailed modeling of the coke combustion therefore requires the coupling of the texture model (Eq. 34), the reaction kinetics (Eqs. 44–46), and a general gas–solid reaction/diffusion model. When the coke particles are considered to be spheres, the following model equations inside the coke pores are obtained.

The continuity equations for oxygen and carbon dioxide are as follows:

$$\frac{\partial}{\partial t}\left[\varepsilon_s (C_{O_2})_s\right] = \frac{1}{r_p^2}\frac{\partial}{\partial r_p}\left[D_{e,O_2} r_p^2 \frac{\partial (C_{O_2})_s}{\partial r_p}\right] - \frac{\rho_{t,0}(1-\varepsilon_{s,0})}{M_C}(R_{C+O_2})_s \quad (48)$$

$$\frac{\partial}{\partial t}\left[\varepsilon_s (C_{CO_2})_s\right] = \frac{1}{r_p^2}\frac{\partial}{\partial r_p}\left[D_{e,CO_2} r_p^2 \frac{\partial (C_{CO_2})_s}{\partial r_p}\right] + \frac{\rho_{t,0}(1-\varepsilon_{s,0})}{M_C}(R_{C+O_2})_s \quad (49)$$

A continuity equation for the coke is also required:

$$\frac{\partial}{\partial t}(\hat{X}_C)_s(r_p, t) = (R_{C+O_2})_s(r_p, t) = \{f[(p_{O_2})_s(r_p, t), T_s]C_{t,0}\} \times [1 - (\hat{X}_C)_s(r_p, t)]\sqrt{1 - \Psi \ln[1 - (\hat{X}_C)_s(r_p, t)]} \quad (50)$$

These equations are simplified by neglecting the accumulation term in the continuity equations for oxygen and carbon dioxide (that is, applying the pseudo-steady state approximation for the gas phase.[33,69,70]

The corresponding initial and boundary conditions are

$$t = 0 \qquad (\hat{X}_C)_s(r_p, t) = 0 \qquad \forall\ r_p \quad (51)$$

$$r_p = 0 \qquad \frac{\partial (C_{O_2})_s(r_p, t)}{\partial r_p} = 0$$

$$\frac{\partial (C_{CO_2})_s(r_p, t)}{\partial r_p} = 0 \qquad \forall\ t \quad (52)$$

$$r_p = r_{p,0} \qquad (C_{O_2})_s = (C_{O_2})_s^s = C_{O_2}$$

$$(C_{CO_2})_s = (C_{CO_2})_s^s = C_{CO_2} \qquad \forall\ t \quad (53)$$

The effective diffusivities of the different components in the pores are calculated following the formula of Bosanquet[71]:

$$\frac{1}{D_{e,i}} = \frac{\tau}{\varepsilon_s}\left(\frac{1}{D_{i,\mathrm{K}}} + \frac{1}{D_{i,m}}\right) \tag{54}$$

in which, according to Dupuit's law, the particle porosity equals the ratio of the pores surface area to the total surface area.[33]

The Knudsen diffusivity can be calculated from

$$D_{i,\mathrm{K}} = \frac{4}{3} r_p \sqrt{\frac{2}{\pi}\frac{RT_s}{M_i}} \tag{55}$$

However, because most of the pores have a diameter of >500 nm, Knudsen diffusion is negligible.

The local porosity is calculated from

$$\varepsilon_s(r_p, t) = \varepsilon_{s,0} + (1 - \varepsilon_{s,0})(\hat{X}_C)_s(r_p, t) \tag{56}$$

with the initial porosity given a value of 0.1 (see Table 1). A typical value of 2.5 is assigned to the coke tortuosity.[72]

The diffusion of the component i in the mixture m is calculated based on the Stefan–Maxwell equation:

$$\frac{1}{D_{i,m}} = \frac{\sum_{j=1}^{n} \frac{x_j N_i - x_i N_j}{D_{ij}}}{N_i - x_i \sum_{j=1}^{n} N_j} \tag{57}$$

In this equation, the binary molecular diffusivities are calculated following the relations of Fuller et al.[73]

The results of the parameter estimation for the kinetic model based on dissociative oxygen adsorption (Eq. 44) and the kinetic model based on associative oxygen adsorption (Eq. 45), in combination with the general gas–solid reaction/diffusion model, are presented in Table 3. For the kinetic model based on dissociative and associative oxygen adsorption (Eq. 46) significantly negative rate constants are obtained and this model is rejected. A further discrimination between the remaining two models is based on the lower residual *SSQ*, the *F*-value, and the smaller individual confidence intervals for the parameters of the model based on dissociative oxygen chemisorption in combination with the general gas–solid reaction/diffusion model. The corresponding parity plot for the selected model is presented in Figure 7. There is a good agreement between the experimentally observed and the model-calculated coke conversions over the entire range of experimental conditions. It can be remarked (not shown) that this was not the case when parity plots were made using the preliminary parameter estimates calculated with the uniform or heterogeneous model. In Figure 8, the calculated total combustion rate, as a function of the oxygen partial pressure, temperature, and coke conversion, is compared with the measured values. A good agreement is obtained under all conditions. In Figures 9 and 10 the coke conversion and the total combustion rate, as a function of time and position in a coke particle, are presented. It follows from these profiles that the limiting models for gas–solid reaction/diffusion, that is, the uniform and the heterogeneous model, cannot adequately describe the experimental observations.

Note that the texture parameter Ψ was estimated not significantly different from zero when the general gas–solid model is used, implying that the effect of the growth of the pores and the overlap of the pores during the coke combustion compensate one another, resulting in a constant internal pore surface area.

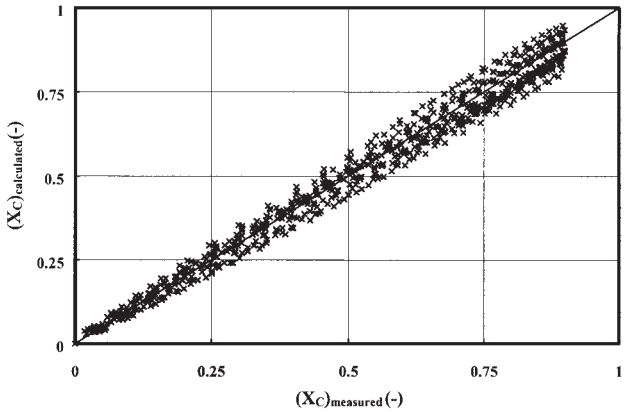

Figure 7. Parity plot for coke conversion by combustion with kinetic model I and general gas–solid reaction/diffusion model.

T = 650–740°C, $(p_{O2})^0$ = 2.1–9.0 kPa.

Finally, the intrinsic rate equation for process gas side coke combustion is

$$R_{C+O_2} = \frac{1007\ \exp\left(-\frac{121{,}399}{RT}\right)\sqrt{p_{O_2}}}{1 + 7.50586510^{-10}\exp\left(\frac{168{,}863}{RT}\right)\sqrt{p_{O_2}}}(1 - X_C) \tag{58}$$

Coke gasification

For the reasons explained earlier, only two steam gasifications of process gas side coke experiments are conducted. The operating conditions are listed in Table 4.

Texture Model. The SEM experiments show that the texture of the pores and the number of active carbon sites during the steam gasification of coke vary with conversion in the same way as during the coke combustion, which implies that the texture model of Bhatia and Perlmutter,[51] with a texture parameter $\Psi = 0$, can be used for the steam gasification of coke as well.

Kinetic Model. In the literature it is generally accepted that the mechanism of steam gasification of coke starts with the dissociative chemisorption of water on a free active carbon site[62,74-78]:

$$C_{fs} + H_2O \underset{k_{-a,d,H_2O}}{\overset{k_{a,d,H_2O}}{\longleftrightarrow}} C(O) + H_2 \tag{59}$$

Semiquinon groups are formed and hydrogen gas is released. According to Chen et al.,[63] the nature of the oxygen complexes that are formed is equal to that of the complexes formed during the coke combustion. In a second step, carbon oxide is formed:

$$C(O) \xrightarrow{k_{sr,d,H_2O}} CO + C_{fs} \tag{60}$$

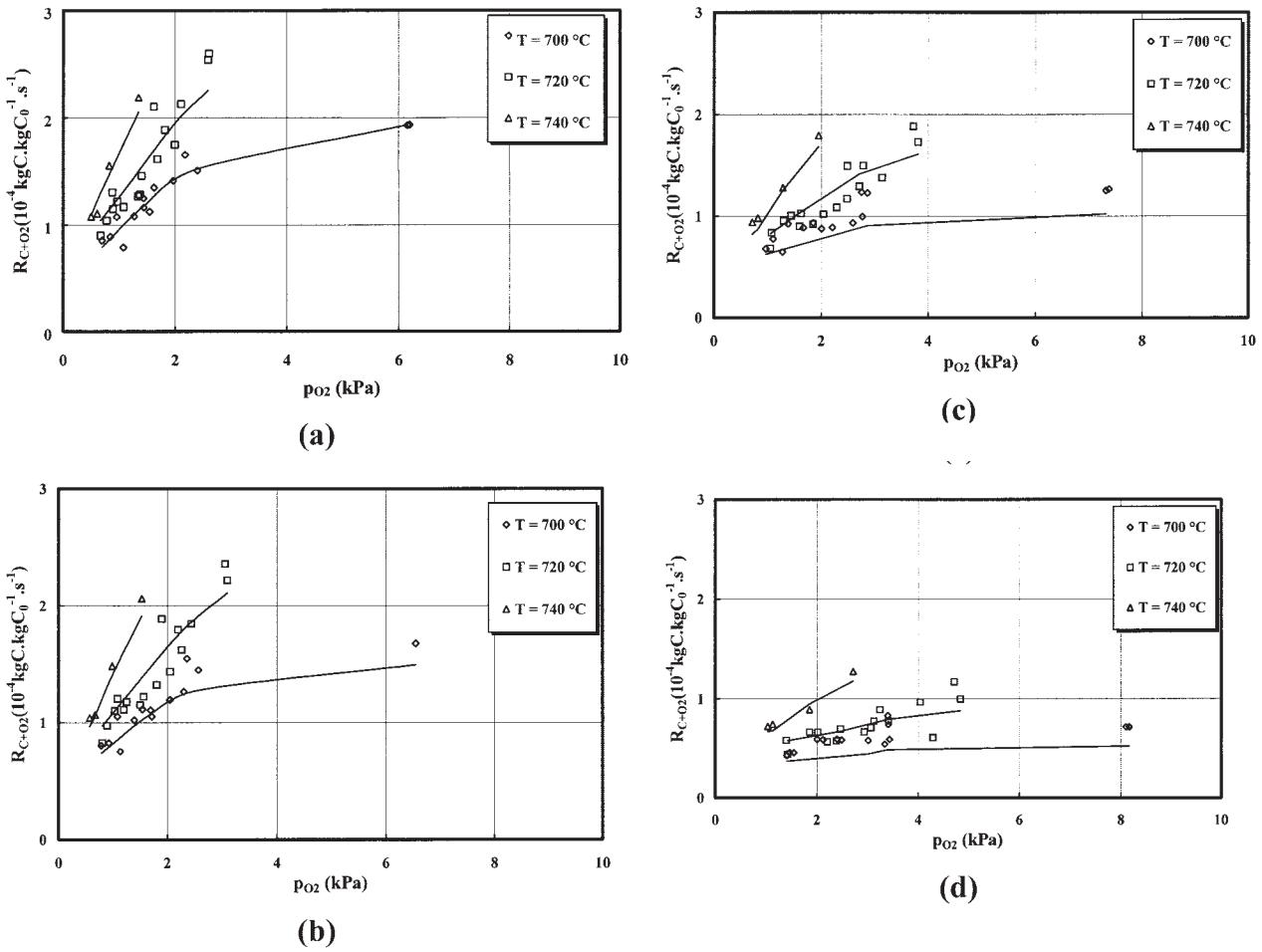

Figure 8. Calculated and measured total rate of coke combustion as a function of oxygen partial pressure at different reaction temperatures and conversions.

(a) $X_C = 20\%$, (b) $X_C = 40\%$, (c) $X_C = 60\%$, (d) $X_C = 80\%$.

The proposed mechanism is completely analogous to that proposed by Laine et al.,[60] except that the chemisorption step (reaction 59) is assumed to be reversible. From the above reaction mechanism, the following reaction rate equation is obtained, under the same assumptions as made for the coke combustion mechanisms:

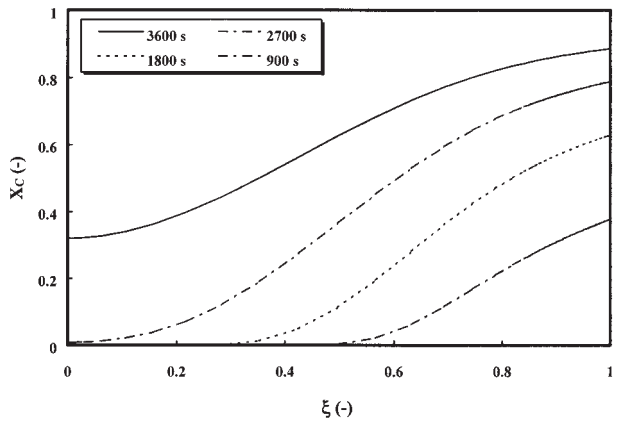

Figure 9. Coke conversion by combustion in the coke particle at different reaction times.

$T = 740$°C, $(p_{O2})^0 = 4.4$ kPa, $W_{C,0}/(F_{O2})^0 = 36.8$ kg C$_0$ s mol^{-1}.

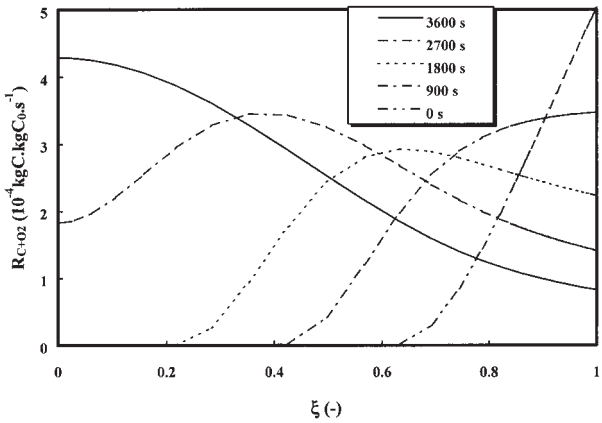

Figure 10. Total rate of coke combustion in the coke particle at different reaction times.

$T = 740$°C, $(p_{O2})^0 = 4.4$ kPa, $W_{C,0}/(F_{O2})^0 = 36.8$ kg C$_0$ s mol^{-1}.

Table 4. Experimental Conditions for Coke Gasification Experiments

N (rpm)	9800
$W_{C,0}$ (10^{-6} kg C_0)	200
T (°C)	880
$W_{C,0}/(F_{H_2O})^0$ (kg C_0 s mol^{-1})	9.1
$(p_{H_2O})^0$ (kPa)	5308
F' (N · μL s)	985

$$R'_{C+H_2O}(t) = \frac{k_{a,d,H_2O} p_{H_2O} C_t(X_C)}{1 + \frac{k_{a,d,H_2O}}{k_{sr,d,H_2O}} p_{H_2O} + \frac{k_{-a,d,H_2O}}{k_{sr,d,H_2O}} p_{H_2}} \quad (61)$$

From several kinetic studies,[28,62,77,78] it was found that the second contribution in the denominator is much smaller than 1 when operating at low total pressures, as is the case for the experiments and for the industrial decoking of crackers. The third term in the denominator can be omitted because negligible amounts of hydrogen gas are detected during the experiments. Under those conditions the intrinsic rate of steam gasification of coke is calculated from

$$R'_{C+H_2O}(t) = k_{a,d,H_2O} p_{H_2O} C_t(X_C) \quad (62)$$

Other mechanisms for the steam gasification of coke at higher pressures can be found in the literature. Because they are of no interest for the decoking of an industrial steam cracker they are not discussed here.

Parameter Estimation. Given that the experimental data are gathered at a constant given partial pressure of steam and a constant temperature (see Table 4), the pressure and temperature dependency of the steam gasification rate cannot be determined from the experimental data. In Eq. 62, the activation energy of the kinetic rate constant is given a value of 238290 J mol^{-1}, taken from the work of Bennet and Price.[15] A uniform gas–solid reaction/diffusion model is used because no internal mass diffusion limitations are calculated for steam. Based on the experimental data obtained in this work, a preexponential factor of 4499 s^{-1} kPa^{-1} is then determined for the given operating conditions, resulting in the following intrinsic rate equation for gasification of the process gas side coke:

$$R_{C+H_2O}(t) = 4491 \exp\left(-\frac{238{,}260}{RT}\right) p_{H_2O}(1 - X_C) \quad (63)$$

Influence of Metals

Some additional experiments are performed with tube metal side coke. For combustion no catalytic effect is found, a phenomenon attributed to the oxidized state of the metal particles during the combustion process. For gasification an initial catalytic activity of reduced Ni particles is seen. However, they are subject to fast deactivation processes, resulting in a rapid reduction of the steam gasification rate as a function of time. Typical profiles are shown in Figure 11.

Conclusions

Kinetic models for the combustion of process gas side coke and tube side coke and for the gasification of process gas side coke are developed by quantitative modeling of a large set of experimental results obtained in an electrobalance experimental setup, especially designed for the experimental research of coke combustion. The combustion and gasification rate are determined from the product of two submodels: one model describes the change of the porous structure and the specific number of active coke sites as a function of coke conversion, using a texture parameter; the second model describes the dependency on the reaction conditions such as partial pressure and temperature.

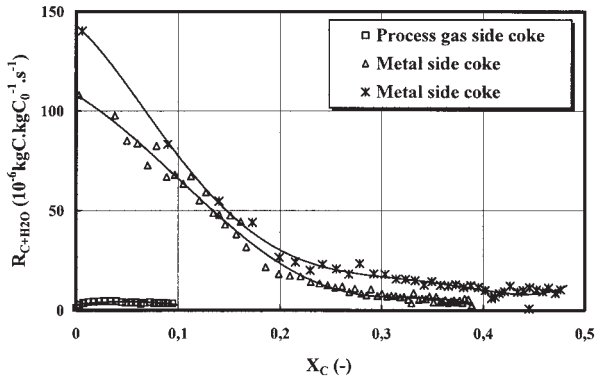

Figure 11. Total rate of gasification as a function of coke conversion by gasification: influence of metal contents of coke.

T = 880°C, $(p_{O2})^0$ = 52.8 kPa, $(p_{N2})^0$ = 50.0 kPa, $(p_{He})^0$ = 3.8 kPa, $W_{C,0}/(F_{H2O})^0$ = 9.1 kg C_0 s mol^{-1}.

Different reaction rate equations, based on a different chemisorption mechanism of the reacting component on the active coke sites, are evaluated for the coke combustion, in combination with different gas–solid reaction/diffusion models. For the coke combustion a kinetic model is selected, corresponding with a dissociative absorption of oxygen on the active coke sites. A general gas–solid reaction/diffusion model, taking into account diffusional limitations for the oxygen in the pores of the coke, is required. The texture parameter was estimated to be zero, implying that the effect of the growth of the pores and the overlap of the pores during the coke combustion compensate each other, resulting in a constant internal pore surface area.

For the coke gasification, the same texture model was used. The gas–solid reaction/diffusion model is a uniform model because no internal mass transport limitations for steam are to be accounted for. The kinetic mechanism is based on the dissociative chemisorption of steam on the active coke sites.

Acknowledgments

The authors acknowledge DSM-The Netherlands and the Fund for Scientific Research–Flanders (FWO-N) "Petrofina Grant" for financial support of this research. G. F. Froment is acknowledged for scientific advice concerning this research.

Notation

A = area, m^2
C_i = concentration of component i in bulk phase, mol m_f^{-3}
CF_i = calibration factor for component i
C_t = specific number of active coke sites, kg C^{-1}
C_t = initial specific number of active coke sites, kg C_0^{-1}
d_p = particle diameter, m_p
$D_{e,i}$ = effective diffusivity of component i in pores, m_f^3 m_p^{-1} s^{-1}

$D_{i,K}$ = Knudsen diffusivity of component i in pores, $m_f^2\ s^{-1}$
$D_{i,m}$ = effective molecular diffusivity of component i in multicomponent mixture in pores, $m_f^2\ s^{-1}$
D_{ij} = binary molecular diffusivity, $m_f^2\ s^{-1}$
F_i = molar flow rate of component i, mol s^{-1}
N_i = molar flux of component i, mol $m_p^{-2}\ s^{-1}$
k_{a,d,O_2} = elementary rate constant for dissociative chemisorption of oxygen, kg C s^{-1} $Pa^{-0.5}$
k_{a,m,O_2} = elementary rate constant for molecular chemisorption of oxygen, kg C s^{-1} Pa^{-1}
k_{sr,d,O_2} = elementary rate constant for C(O) complex disintegration, kg C s^{-1}
k_{sr,m,O_2} = elementary rate constant for $C(O_2)$ complex disintegration, kg C s^{-1}
L = characteristic particle length, m_p
L_m = specific pores length of the coke, m_s kg C^{-1}
M_i = molecular mass of component i, kg mol^{-1}
$\dot{m}_i$ = mass flow rate of component i, kg s^{-1}
Nu = Nusselt number
p_i = partial pressure of component i, Pa
p_t = total pressure, Pa
Pr = Prandtl number
R = gas constant, J $mol^{-1}\ K^{-1}$
R_i = rate of formation/consumption of component i, mol kg C_0^{-1} s^{-1}
R_{C+O_2} = total coke combustion rate kg C kg $C_0^{-1}\ s^{-1}$
R'_{C+O_2} = specific coke combustion rate, kg C kg $C^{-1}\ s^{-1}$
R_{C+H_2O} = total coke gasification rate, kg C kg $C_0^{-1}\ s^{-1}$
R'_{C+H_2O} = specific coke gasification rate, kg C kg $C^{-1}\ s^{-1}$
Re = Reynolds number
r_p = particle radius, m_p
S = selectivity
S_m = specific pores surface area of the coke, m_s^2 kg C^{-1}
S_V = volumetric pores surface area of the coke, $m_s^2\ m_p^{-3}$
Sc = Schmidt number
Sh = Sherwood number
SSQ = sum of squares
T = temperature, K
t = time, s
V = volume, m^3
W_C = mass, kg C
w_i = weight fraction of component i
x_i = mole fraction of component i
X_C = coke conversion, kg C kg C_0^{-1}

Greek letters

ε_s = porosity, $m_f^3\ m_p^{-3}$ (in Eq. 55, $m_f^2\ m_p^{-2}$)
ΔH = reaction enthalpy, J $mol^{-1}\ K^{-1}$
λ_C = thermal conductivity of coke, J $m^{-1}\ K^{-1}\ s^{-1}$
λ = number of active coke sites per unit surface area, m_s^{-2}
τ = tortuosity, $m_f\ m_p^{-1}$
ξ = relative position inside particle
ϕ = Thiele modulus
Φ = Weisz modulus
ρ_p = particle density, kg C m_p^{-3}
ρ_t = coke density (without pores), kg C m_s^{-3}
Ψ = texture parameter

Subscripts

a = chemisorption
C = carbon
d = dissociative
e = effective
f = fluid
fs = free site
i = component i
m = molecular
obs = observed (for uniform and heterogeneous shrinking core model)
p = particle
r = reactor
ref = reference component
s = solid
t = total
0 = initial value

Superscripts

s = surface
^ = calculated value
0 = at the reactor inlet

Literature Cited

1. Ranzi E, Dente M, Pierucci S, Biardi G. Initial product distribution from pyrolysis of normal and branched paraffins. *Ind Eng Chem Fundam.* 1983;22:132.
2. Dente M, Ranzi E. *Pyrolysis: Theory and Industrial Practice*. San Diego, CA: Academic Press; 1983.
3. Willems P, Froment GF. Kinetic modeling of the thermal cracking of hydrocarbons. Part 1: Calculation of frequency factors. *Ind Eng Chem Res.* 1988a;27:1959.
4. Willems P, Froment GF. Kinetic modeling of the thermal cracking of hydrocarbons. Part 2: Calculation of activation energy. *Ind Eng Chem Res.* 1988b;27:1966.
5. Kopinke F-D, Zimmerman G, Reyniers GC, Froment GF. Relative rates of coke formation from hydrocarbons in steam cracking of naphtha. 2. Paraffins, naphthenes, mono-, di-, and cyclo-olefines, and acetylene. *Ind Eng Chem Res.* 1993a;32:56.
6. Kopinke F-D, Zimmerman G, Reyniers GC, Reyniers M-F, Froment GF. Relative rates of coke formation from hydrocarbons in stream cracking of naphtha. 3. Aromatic hydrocarbons. *Ind Eng Chem Res.* 1993b;32:2620.
7. Reyniers GC, Froment GF, Kopinke F-D, Zimmerman G. Coke formation in the thermal cracking of hydrocarbons. *Ind Eng Chem Res.* 1994;33:2584.
8. Wauters S, Marin GB. Computer generation of a network of elementary steps for coke formation during the thermal cracking of hydrocarbons. *Chem Eng J.* 2001;82:267.
9. Wauters S, Marin GB. Kinetic modeling of coke formation during steam cracking. *I&EC Res.* 2002;41:2379.
10. Van Speybroeck V, Van Neck D, Waroquier M, Wauters S, Saeys M, Marin GB. Ab initio study on the elementary radical reactions in coke formation. *Int J Quantum Chem.* 2003;91:384.
11. Rao MV, Plehiers PM, Froment GF. The coupled simulation of heat transfer and reaction in a pyrolysis furnace. *Chem Eng Sci.* 1988;43:1223.
12. Heynderickx GJ, Froment GF. A pyrolysis furnace with reactor tubes of elliptical cross section. *Ind Eng Chem Res.* 1996;35:2183.
13. Schools EM, Froment GF. Simulation of decoking of thermal cracking coils by steam/air mixtures. *AIChE J.* 1997;43:118.
14. Heynderickx GJ, Froment GF. Simulation and comparison of the run length of an ethane cracking furnace with reactor tubes of circular and elliptical cross section. *Ind Eng Chem Res.* 1998;37:914.
15. Bennet MJ, Price JB. A physical and chemical examination of an ethylene steam cracker coke and of the underlying pyrolysis tube. *J Mater Sci.* 1981;16:170.
16. Kim MS, Rodriguez NM, Baker RTK, Milks D. Electron microscopy characterization studies of carbon deposits formed during steam cracking of ethane. Symp on Coke Formation and Mitigation; 1995:618.
17. Albright LF, Marek JC. Coke formation during pyrolysis: Roles of residence time, reactor geometry, and time of operation. *Ind Eng Chem Res.* 1988a;27:743.
18. Albright LF, Marek JC. Analysis of coke produced in ethylene furnaces: Insights on process improvements. *Ind Eng Chem Res.* 1988b;27:751.
19. Albright LF, Marek JC. Mechanistic model for formation of coke in pyrolysis units producing ethylene. *Ind Eng Chem Res.* 1988c;27:755.
20. Marchand A. Physico-chemical and structural characterization of carbons. In: Figueiredo JL, Moulijn JA, eds. *Carbon and Coal Gasifications*. NATO ASI Sub-Series E Applied Sciences 105. Dordrecht, The Netherlands: Kluwer Academic Publishers B.V.; 1986:93.
21. Jackson PRS, Young DJ, Trimm DL. Coke deposition on and removal from metals and heat-resistant alloys under steam cracking conditions. *J Mater Sci.* 1986;21:4276.
22. Baker RTK, Barber MA, Harris PS, Feates FS, Waite RJ. Nucleation and growth of carbon deposits from the nickel catalyzed decomposition of acetylene. *J Catal.* 1972;26:51.

23. Baker RTK, Harris PS, Thomas RB, Waite RJ. Formation of filamentous carbon from iron and chromium catalyzed decomposition of acetylene. *J Catal.* 1973;30:86.
24. Bernardo CA, Lobo LS. Kinetics of carbon formation from acetylene on nickel. *J Catal.* 1975;37:267.
25. Figueiredo JL. Filamentous carbon. *Erdöl Kohle-Erdgas-Petrochem.* 1989;42:294.
26. Lahaye J, Badie P, Ducret J. Mechanism of carbon formation during steam cracking of hydrocarbons. *Carbon.* 1977;15:87.
27. Trimm DL. The formation and removal of coke from nickel catalysts. *Catal Rev Sci Eng.* 1977;16:155.
28. Bennet MJ, Price JB. Oxidation of ethylene steam cracker pyrolysis tune deposits in water vapor and its enhancement by inorganic catalysts. In: Albright LF, Baker RTK, eds. *Coke Formation on Metal Surfaces*. ACS Symposium Series 202, Washington, DC: American Chemical Society; 1982:59.
29. Wakao N, Funazkri T. Effect of fluid dispersion coefficients on particle-to-fluid mass transfer coefficients in packed bed. *Chem Eng Sci.* 1978;33:1375.
30. Kaguei S, Matsumoto K, Wakao N. Effect of dead volume on estimation of packed bed parameters from input–output response curves. *Chem Eng Sci.* 1980;35:1809.
31. Wakao N, Kaguei S, Funazkri T. Effect of fluid dispersion coefficients on particle-to-fluid heat transfer coefficients in packed bed. *Chem Eng Sci.* 1979;34:325.
32. Weisz PB, Prater CD. Interpretation of measurements in experimental catalysis. *Adv Catal.* 1954;6:143.
33. Froment GF, Bischoff KB. *Chemical Reactor Analysis and Design*. New York, NY: Wiley; 1990.
34. Froment GF, Hosten LH. Catalytic kinetics: Modeling. In: *Catalysis, Science and Technology*. Vol. 2. Berlin: Springer-Verlag; 1981.
35. Bhatia SK, Perlmutter DD. A random pore model for fluid–solid reactions: II. Diffusion and transport effects. *AIChE J.* 1981;27:247.
36. Suuberg EM. Thermal induced changes in reactivity of carbons. In: Lahaye J, Ehrburger P, eds. *Fundamental Issues in Control of Carbon Reactivity*. NATO ASI Sub-Series E Applied Sciences 192. Dordrecht, The Netherlands: Kluwer Academic Publishers B.V.; 1991:269.
37. Szekely J, Evans JW. A structural model for gas–solid reactions with a moving boundary. *Chem Eng Sci.* 1970;25:1091.
38. Szekely J, Evans JW. A structural model for gas–solid reactions with a moving boundary—II. The effects of grain size, porosity and temperature on the reactions of porous pellets. *Chem Eng Sci.* 1971;26:1901.
39. Sohn HY, Szekely J. A structural model for gas–solid reactions with a moving boundary—III. A general dimensionless representation of the irreversible reaction between a porous solid and a reactant gas. *Chem Eng Sci.* 1972;27:763.
40. Sohn HY, Szekely J. A structural model for gas–solid reactions with a moving boundary—IV. Langmuir–Hinshelwood kinetics. *Chem Eng Sci.* 1973;28:1169.
41. Park JY, Levenspiel O. The crackling core model for the reaction of solid particles. *Chem Eng Sci.* 1975;30:1207.
42. Szekely J, Propster P. A structural model for gas–solid reactions with a moving boundary—VI. The effects of grain size distribution on the conversion of porous solids. *Chem Eng Sci.* 1975;30:1049.
43. Adschiri T, Furusawa T. Estimation of dynamic change in gasification rate of chars—I. A common formulation of dynamic change in experimentally observed surface area during steam gasification of char. *Chem Eng Sci.* 1987;42:1313.
44. Adschiri T, Kojima T, Furusawa T. Estimation of dynamic change in gasification rate of chars—II. Overlapped grain model. *Chem Eng Sci.* 1987;42:1319.
45. Sotirchos SV. On a class of random pore and grain models for gas–solid reactions. *Chem Eng Sci.* 1987;42:1262.
46. Petersen EE. Reaction of porous solids. *AIChE J.* 1957;3:443.
47. Hashimoto K, Silveston PL, Gasification: Part I. Isothermal kinetic control model for a solid with a pore size distribution. *AIChE J.* 1973;19:259.
48. Simons GA, Finson ML. The structure of coal char: Part 1. Pore branching. *Combust Sci Technol.* 1979;42:217.
49. Simons GA. The structure of coal char: Part 2. Pore combination. *Combust Sci Technol.* 1979;42:227.
50. Simons GA. The unified coal-char reaction. *Fuel.* 1980;59:143.
51. Bhatia SK, Perlmutter DD. A random pore model for fluid–solid reactions: I. Isothermal kinetic control. *AIChE J.* 1980;26:379.
52. Gavalas GR. A random capillary model with application to char gasification at chemically controlled rates. *AIChE J.* 1980;26:577.
53. Delikouras EA, Perlmutter DD. Inaccessible porosity in gasification reactions under kinetic control. *AIChE J.* 1991;37:1607.
54. Delikouras EA, Perlmutter DD. Combined effects of mass transfer and inaccessible porosity in gasification reactions. *AIChE J.* 1993;39:829.
55. Reyes S, Jensen KF. Percolation concepts in modeling of gas–solid reactions—I. Application to char gasification in the kinetic regime. *Chem Eng Sci.* 1986a;41:333.
56. Reyes S, Jensen KF. Percolation concepts in modeling of gas–solid reactions—II. Application to char gasification in the diffusion regime. *Chem Eng Sci.* 1986b;41:345.
57. Shah N, Ottino JM. Transport and reaction evolving disordered composites—I. Gasification of porous solids. *Chem Eng Sci.* 1987;42:63.
58. Fuertes AB, Marban G. Modeling gasification reactions including the percolation phenomenon. *Chem Eng Sci*. 1994;49:3813.
59. Marban G, Fuertes AB. Influence of percolation on the modification of the overall particle properties during gasification of porous solids. *Chem Eng Sci.* 1997;52:1.
60. Laine NR, Vastola FJ, Walker PL. The importance of active surface area in the carbon–oxygen reaction. *J Phys Chem.* 1963;67:2030.
61. Blyholder G, Ehring H. *J Phys Chem.* 1959;63:1004.
62. Laurendeau NM. Heterogeneous kinetics of coal char gasification and combustion. *Prog Energy Combust Sci.* 1978;4:221.
63. Chen SG, Yang RT, Kapteijn F, Moulijn JA. A new surface oxygen complex on carbon: Towards a unified mechanism for carbon gasification reactions. *Ind Eng Chem Res.* 1993;32:2835.
64. Li YH, Lu GQ, Rudolph V. The kinetics of NO and N_2O reduction over coal chars in fluidized-bed combustion. *Chem Eng Sci.* 1998;53:1.
65. Essenhigh RH. *Fundamentals of Coal Combustion. Chemistry of Coal Utilization*. Vol. 19, 2nd Suppl. New York, NY: Wiley; 1981.
66. Walker PL, Taylor RL, Ranish JM. An update on the carbon oxygen reaction. *Carbon.* 1991;29:411.
67. Du Z, Sarofim AF, Longwell JP. The CO–CO_2 ratio in the products of the carbon-oxygen reaction. In: Lahaye J, Ehrburger P, eds. *Fundamental Issues in Control of Carbon Reactivity*. NATO ASI Sub-Series E Applied Sciences 192. Dordrecht, The Netherlands: Kluwer Academic Publishers B.V.; 1991a:91.
68. Du Z, Sarofim AF, Longwell JP, Mims CA. Kinetic measurements and modeling of carbon oxidation. *Energy Fuels.* 1991b;5:214.
69. Bischoff KB. Accuracy of the pseudo steady state approximation for moving boundary problems. *Chem Eng Sci.* 1963;18:711.
70. Bhatia SK. On the pseudo steady state hypothesis for fluid–solid. *Chem Eng Sci.* 1985;40:868.
71. Satterfield CN. *Mass Transfer in Heterogeneous Catalysis*. Cambridge, MA: MIT Press; 1970.
72. Bliek A, Lont JC, van Swaaij PM. Gasification of coal-derived chars in synthesis gas mixtures under intraparticle mass-transfer-controlled conditions. *Chem Eng Sci.* 1986;41:1895.
73. Reid RC, Prausnitz JM, Poling BE. *The Properties of Gases and Liquids*. 4th ed. New York, NY: McGraw-Hill; 1988.
74. Walker PL, Rusinko F, Austin LG. Gas reaction of carbon. In: Eley DD, Selwood PW, Weisz PB, eds. *Advances in Catalysis*. New York, NY: Academic Press; 1959.
75. Ergun S. Kinetics of the reaction of carbon dioxide and steam with coke. USBM Bulletin 598. Washington, DC: U.S. Bureau of Mines; 1962:38.
76. Giberson RC, Walker JP. Reaction of nuclear graphite with water vapor. 1. The effect of hydrogen and water vapor partial pressures. *Carbon.* 1966;3:521.
77. Johnson JL. Fundamentals of coal gasification. In: *Kinetics of Coal Gasification*. New York, NY: Wiley; 1979.
78. Hüttinger KJ, Lietzke GA. Mechanismen und kinetik der wasserdampfvergassung. Rolle der wasserstof-inhibierung—Teil I. *Erdöl Kohle-Erdgas-Petrochem.* 1989;42:241.

Manuscript received Mar. 5, 2004, and revision received Sept. 3, 2004.